Contents lists available at ScienceDirect

Materials Today Bio

journal homepage: www.journals.elsevier.com/materials-today-bio

Coaxial electrospun Ag-NPs-loaded endograft membrane with long-term antibacterial function treating mycotic aortic aneurysm

Qingxi Hu [a,b,c], Zhenwei Huang [a], Haiguang Zhang [a,b,c,*], Pengcheng Ma [e,**], Rui Feng [d,***], Jiaxuan Feng [f,****]

[a] Rapid Manufacturing Engineering Center, School of Mechatronic Engineering and Automation, Shanghai University, Shanghai, 200444, China
[b] Shanghai Key Laboratory of Intelligent Manufacturing and Robotics, Shanghai University, Shanghai, 200072, China
[c] National Demonstration Center for Experimental Engineering Training Education, Shanghai University, Shanghai, 200444, China
[d] Shanghai General Hospital, Shanghai Jiaotong University, Shanghai, China
[e] Department of Vascular Surgery, Changhai Hospital, Naval Medical University, Shanghai, 200433, China
[f] Vascular surgery department, Ruijin Hospital, affiliated to Medical school of Shanghai Jiaotong University, Shanghai, PR China

ARTICLE INFO

ABSTRACT

The use of endovascular stent-graft has become an important option in the treatment of aortic pathologies. However, the currently used endograft membranes have limited ability to prevent bacterial colonization. This makes them unsuitable for the treatment of mycotic aneurysms, as the infection is prone to progress after endograft implantation. Moreover, even in non-mycotic aortic pathologies, endograft infections can occur in the short or long term, especially for patients with diabetes mellitus or in immune insufficiency conditions. So, this study aimed to develop a kind of Ag-NPs-loaded endograft membrane by coaxial electrospinning technique, and a series of physical and chemical properties and biological properties of the Ag-NPs-loaded membrane were characterized. Animal experiments conducted in pigs confirmed that the Ag-NPs-loaded membrane was basically non-toxic, exhibited good biocompatibility, and effectively prevented bacterial growth in a mycotic aortic aneurysm model. In conclusion, the Ag-NPs-loaded membrane exhibited good biocompatibility, good anti-infection function and slow-release of Ag-NPs for long-term bacteriostasis. Thus, the Ag-NPs-loaded membrane might hold potential for preventing infection progression and treating mycotic aortic aneurysms in an endo-vascular way.

1. Introduction

Endovascular treatment has become an important option to treat aortic aneurysms. This procedure used a covered stent to exclude the aortic pathologies. It consists of nitinol stent skeleton and artificial vascular membrane. The materials for the vascular membrane were polyethylene terephthalate (PET) and expanded polytetrafluoroethylene (ePTFE) [1,2]. Bacterial infection of the endograft has been a major threat after the endovascular procedure, especially when the stent-graft was implanted in mycotic aortic aneurysm [3–5]. Infections of the endograft can occur shortly after the procedure or even years later [6].

Researchers have been investigating different ways to incorporate antibacterial capacity into the stent graft. The development of a drug-loaded membrane can improve antibacterial ability of the stent-graft. In recent years, various strategies have been developed, including the use of drug-loaded membrane prepared by pulsed laser deposition (PLD) technique [7], modifying the surface of membrane through layer-by-layer (LBL) assembly or blend electrospinning [8]. However, these methods caused the drugs to adhere to the surface of membrane, which may lead to a burst release of drug and the inability to extend the

duration of drug action [9]. The application of electrospun nanofibers in drug delivery system offers targeted drug delivery, sustained release, rapid onset and good pharmacokinetics [10]. This technology has been widely applied in the biomedical field.

Biomolecular materials, such as Polycaprolactone (PCL), Polyactic acid (PLA) and Polytetrafluoroethylene (PTFE), are usually selected in the preparation of membranes of the stent-graft by electrospinning, but these materials possess different characteristics. PCL is a biodegradable polymer widely employed in the biomedical field due to its excellent mechanical properties and biocompatibility [11,12]. Nevertheless, as a relatively hydrophobic material, PCL has poor cell affinity, which is not conducive to cell adhesion [13]. Chitosan is a natural polysaccharide extracted from the chitin N-diacetyl group. It has good hydrophilicity, biodegradability, non-toxicity, and antibacterial properties and can be used to improve the hydrophilicity of PCL [14–16]. In addition, chitosan is difficult to electrospin due to its low solubility and high viscosity, necessitating the use of blending and grafting methods to improve its spinnability. Duan [17]et al. found that adding an appropriate amount of polyoxyethylene (PEO) to the acetic acid solution of chitosan significantly improved its spinnability and performance in coaxial electrospinning.

Chitosan can be used to load antibacterial drugs [18–20], such as Amoxicillin, Penicillin, Vancomycin and Silver nanoparticles (Ag-NPs). Ag-NPs is a classic antibacterial agent, that has been studied for many years for its dose-dependent toxicity and promising antibacterial activity [21–23]. The combination of chitosan and Ag-NPs has long been studied for medical applications, as it is more effective against bacteria than pure chitosan. Moreover, chitosan can serve as a stabilizer to prevent the aggregation of Ag-NPs [24].

This study aims to develop an Ag-NPs-loaded membrane via coaxial electrospinning. The prepared Ag-NPs-loaded membrane has core-shell nanofibers, with Ag-NPs wrapped in the core layer of nanofibers, effectively controlling the release rate of Ag-NPs. Then the physicochemical properties, antibacterial properties and drug release properties of the Ag-NPs-loaded membrane were evaluated. The biocompatibility and feasibility of the Ag-NPs-loaded membrane were demonstrated through in vitro and in vivo experiments.

2. Materials and methods

2.1. Preparation of the Ag-NPs-loaded membrane

PCL (MW = 80,000 g/mol) was supplied by Solvay S.A.(Belgium), and a solution of silver nanoparticles (10000 ppm) was purchased from Mingcheng Plastic Additives Chemical Co. Ltd (Dongguan, China). CS (molecular weight: approximately 300 kDa; degree of deacetylation:80–95 %), PEO (molecular weight: approximately 600 kDa), Dichloromethane (DCM), N,N-Dimethylformamide (DMF)and Acetic acid (HAc) were all purchased from Sinopharm Chemical Reagent Co. Ltd (Shanghai, China). All materials were of analytical grade and used as received.

By using a coaxial needle, the two components can be fed separately through the inner and outer coaxial capillary channels and integrated into the core/shell structure of the composite fiber [25,26].Firstly, the shell solution was prepared by dissolving PCL in DCM/DMF(7:3, v/v) and stirring for 4 h at room temperature. The solution with a PCL concentration of 15 wt% was prepared and used as the shell layer. Secondly, CS and PEO were separately dissolved in two different Hac solutions to prepare CS and PEO solutions with a concentration of 3 wt% for each of them. After stirring separately at room temperature for 6 h, the two solutions were mixed, and Ag-NPs were added and stir for another 4 h. The mixed solution containing Ag-NPs was used as the core layer, with the concentration of Ag-NPs set at 1 wt%, 2 wt% and 3 wt% for comparison. The preparation process is illustrated in Fig. 1, and the components in coaxial electrospinning solutions are shown in Table 1.

The diameter of the coaxial needle was 1.0 mm for the shell polymer and 0.4 mm for the core polymer. The core and shell solutions were loaded into 10 mL syringes and controlled by two syringe pumps, with the shell needle connected to the syringe through a Teflon capillary catheter. The liquid supply velocity of the core was set as 0.2 mL/h, and the liquid supply velocity ratios of the core and shell were set at 1:3, 1:2 and 1:1 for comparison. Applied a voltage of 15 kV to the coaxial needle and set the speed of the drum receiver to 200 r/min. The distance between the coaxial needle and the drum receiver was 15 cm, the ambient temperature was 30 °C, and the humidity was 40 %. After 8 h of electrospinning, the Ag-NPs-loaded membrane was removed from the drum receiver and placed in an electric heating blast drying oven (GZX-9070MBE, China). It was dried at 40 °C for 24 h to remove the surface solvent. A macroscopic view of Ag-NPs-loaded membrane was shown in

Table 1
Components in coaxial electrospinning solutions.

Samples	Core			Shell
	CS(w/v)	PEO(w/v)	Ag-NPs(w/v)	PCL(w/v)
I	3 %	3 %	1 %	15 %
II	3 %	3 %	2 %	15 %
III	3 %	3 %	3 %	15 %
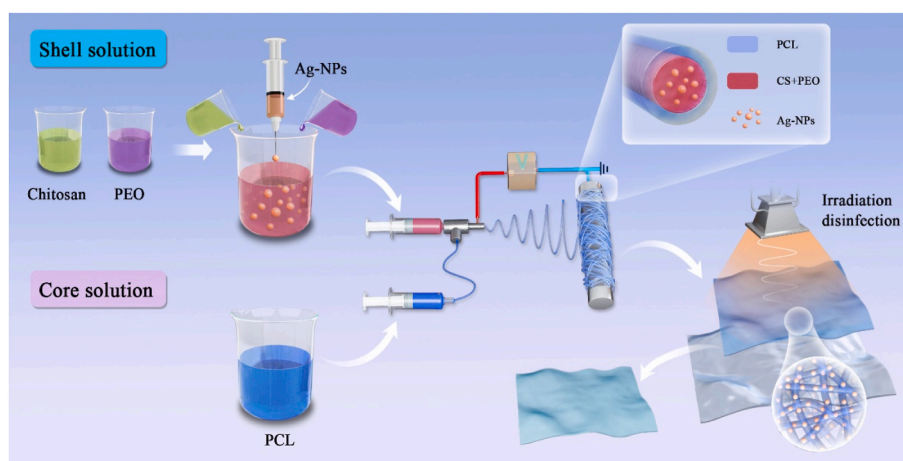
Fig. 1. Experimental procedure. First, CS and PEO were dissolved in solvent (Acetic acid), after the solutions were completely dissolved, the two solutions were mixed and the Ag-NPs solution was added. PCL was dissolved in mixed solvent (DCM and DMF, at a 7:3 vol ratio); Ag-NPs-loaded membrane of fibers with core-shell structure prepared by coaxial electrospinning, then the Ag-NPs-loaded membrane was irradited and disinfected.

Fig. 4(a).

2.2. Characterization methods

1. Scanning Electron Microscope (SEM) analysis

The morphology of the Ag-NPs-loaded membrane was observed via SEM (HITACHI SU-1500, Japan). The membranes were cut into 10 mm × 5 mm pieces and pasted onto the copper grids, which was sprayed with gold before observation. Used Nano Measurer software to measure the fibers' diameter and then analyzed the frequency distribution of fibers. Energy spectrum analysis was also performed to detect whether Ag-NPs were present in the fibers.

2. Transmission Electron Microscopy (TEM) Analysis

Hold the 230-mesh carbon-coated copper grid with small tweezers and shake it approximately 15 cm away from the coaxial needle for 1 min during the electrospinning process, and then coaxial electrospun fibers were deposited on the copper grid. Applying an accelerating voltage of 100 kV to the copper grid with TEM (Hitachi HT7800, Japan) and then taking TEM images to observe whether the core-shell structure was formed.

3. Fourier Transform infrared spectroscopy (FTIR)

The chemical composition of Ag-NPs-loaded membranes was analyzed by an infrared spectrometer (FT-IR 370, China). PCL, CS and PEO were ground into a fine enough powder, which was then diluted with Potassium Cyanide and a small sample was placed into the machine for testing. A small amount of Ag-NPs liquid was placed in two CaF2 cover slides and put into machine for testing. The membranes were pressed by a press until they were thin enough and then tested. Each spectrum was obtained with a resolution of 2 cm^{-1} and a wave number range of 4000 to 500 cm^{-1}.

4. Mechanical Properties

The Ag-NPs-loaded membranes were cut into rectangles of 50 mm × 10 mm, clamp the membranes with the two ends of the material testing machine (WDW-1, Z2.5/TSIS 200Pro, Germany) and apply a 0.1 kN pre-tightening force, stretch it at 10 mm/min until the membranes breaks, take three samples from each Ag-NPs-loaded membrane and take the average value as the final result, then the tensile strength and elastic modulus were introduced to quantify the mechanical properties of membranes, which are defined by the following formula:

$$\text{Tensile strength} = \frac{F}{A}$$

$$\text{Elastic modulus} = \frac{F/A}{dL/L}$$

where F represents the maximum force that the membrane can withstand at the yield stage, A represents the original cross-sectional area of the membrane, dL represents the elongation of the membrane, and L represents the original length of membrane.

5. Contact Angle (CA) Measurements

The contact angle value of the Ag-NPs-loaded membranes was measured by a water contact angle measuring instrument (OCA 15 EC, China). Take five samples from each electrospun membrane and the water contact angle was measured at 30 s, and take the average value as the final result.

2.3. Antibacterial experiment

The antibacterial activities of Ag-NPs-loaded membranes were tested in vitro by evaluating their inhibitory effect on *Escherichia coli* (*E. coli*) and staphylococcus aureus (*S. aureus*). The Ag-NPs-loaded membranes containing different concentrations of Ag-NPs were cut into square pieces measuring 1 × 1 cm. Each membrane was placed on solid petri dishes evenly coated with 30 μL *E. coli* or *S. aureus*, and the concentration of bacteria (*E. coli* and *S. aureus*) is approximately 10^8 CFU/ml. The petri dishes were then incubated at 37 °C for 24 h, 72 h and 120 h. After incubation, the bacteriostatic circles were observed and measured.

2.4. Silver ions release

The absorbance of Ag-NPs was measured by a spectrometer, and the standard curve was constructed. The Ag-NPs-loaded membranes to be tested were placed in centrifuge tubes filled with 50 mL phosphate buffer. After soaking for 4 h, 8 h, 12 h, 24 h, 48 h and 72 h until 192 h, the appropriate amount of solution to be measured was taken and the same amount of fresh phosphate buffer was added. The absorbance of obtained solution was measured by a spectrophotometer. Then the release rate of Ag-NPs was calculated based on the standard curve.

2.5. In vitro cell experiment

1. Cytotoxicity test

The cytotoxicity of Ag-NPs-loaded membranes was detected using the Cell Counting Kit-8(CCK-8, Service) as a previously reported approach [27]. Human Umbilical Vein Endothelial Cells (HUVECs) were selected as the cell type for the experiment, the cell suspension was prepared using a treated medium at a cell density of 1×10^5 cells/ml. Subsequently, 100 μL of the cell suspension was seeded in each well of a 96-well plate. After 1, 3 and 5 days of incubation, 10 μL of CCK-8 kit was added into each well and placed in a humidified incubator for 4 h. Fresh medium and PCL-prepared membrane were included as a control group. The OD values were measured at wavelengths of 450 nm using a microplate reader (Tecan Group Ltd., Switzerland).

2. Cell adhesion

In order to evaluate the cytocompatibility and potential cytotoxicity of the Ag-NPs-loaded membranes, they were seeded in HUVECs. In brief, the Ag-NPs-loaded membranes were immersed into 75 % ethanol for 1 h, then membranes were removed and rinsed tree times with PBS. Finally, membranes were immersed into fresh medium under UV light for 4 h before inoculation. The prepared cell suspension(1×10^6 cells/mL) was poured into petri dishes containing membrane until the membrane is completely covered, which were then placed into humidified incubator for 4 h.After cell adhesion, fresh medium was added into dishes until the surface of membranes were covered, then moved them into the incubator for cultivation at 37 °C in 5 % CO_2, with the culture medium refreshed everyday thereafter. After 1, 3 and 5 days of incubation, cell proliferation and growth were evaluated by live/dead staining. Live and dead cells were stained by calcein (Calcein AM) and PI, membranes were mounted on microscope slides for observation using an inverse fluorescence microscope (Eclipse Ti–U, Nikon Instruments Inc., Japan) at 1, 3 and 5 days, and then captured representative fluorescent images.

2.6. In vivo experiment in animal models of mycotic aortic aneurysms

Glutaraldehyde-treated bovine pericardium was kept in saline. The Ag-NPs-loaded membrane were sewn on the outer side of iliac extention stent-grafts (16-16-60 mm, Shanghai MicroPort Medical (Group) Co., Ltd., China), which were used as exclusion endo-device. All the experimental materials and devices are sterilized by irradiation. 9 white pigs

(Specific name: Shanghai white pig), each weighing approximately 60 kg, were divided into 3 groups (Fig. 2). The experimental protocol was established, according to the ethical guidelines of the Helsinki Declaration and was approved by the Human Ethics Committee of Shanghai Changhai Hospital Ethics Committee. Written informed consent was obtained from individual or guardian participants. General anesthesia with tracheal intubation was adopted. The glutaraldehyde-treated bovine pericardium was cut and sewn in the shape of a pocket, with an opening length of 4.0 cm. A median abdominal incision was made to expose the infrarenal abdominal aorta. After general heparinization, the infrarenal abdominal aorta was clamped. The anterior wall of the middle segment of the infrarenal abdominal aorta was incised longitudinally for 4.0 cm. The open of the pocket-shaped bovine pericardium was sutured to the incision of the abdominal aorta with continuous sutures. So, the abdominal aorta aneurysm was formed (Fig. 3).

Abdominal aortography was performed in the manner of "Flow speed: 15 ml/s, Volumn: 25 ml, Pressure: 800PSI. Contrast: Iodixanol (GE Healthcare, USA)". (Fig. 3 a2). The stent-graft was resheathed into the delivery system, and was delivered along the extra-stiff guidewire to the ideal location of abdominal aorta aneurysm. It was deployed with sufficient proximal and distal landing zone. Final arteriography was conducted to confirm the complete exclusion of the aneurysm.

Then bacterial solution injection was then injected into the aneurysm sac. There were three groups of pigs: the aneurysms of group 1 were treated by conventional stent-graft, and were injected with 1.0 ml of *E. coli* and *S. aureus*; the aneurysms of group 2 were treated by the stent-graft covered by Ag-NPs-loaded membrane, and were injected with 1.0 ml of *E. coli*; the aneurysms of group 3 were treated by the stent-graft covered by Ag-NPs-loaded membrane, and were injected with 1.0 ml of *S. aureus* [28].

After the procedure, the pigs were administrated with ceftriaxone sodium and penicillin for 1 week. They were fed for 1 month, and then euthanized. After euthanasia, the infrarenal abdominal aorta, aortic aneurysm, and implanted stent-grafts were collected as a whole. Gross observations, HE staining and Gram staining were performed.

2.7. Statistical analysis

All characterizations were analyzed using Origin, Nano Measurer and ImageJ software. The results were expressed as mean ± SD (standard deviation), Analysis of variance (Anova) and student's t-test were used to reveal statistical differences between result.

3. Results

3.1. Characterization of membrane microstructure

As shown in Fig. 4(b–d), b, c and d are nanofibers of Ag-NPs-loaded membranes prepared with core-shell liquid supply ratios of 1:3,1:2 and 1:1. The normal statistical graph of diameter distribution of three kinds of nanofibers also is shown in Fig. 4(b1-d1). The diameter of three kinds of nanofibers was 530 ± 88 nm,510 ± 89 nm,520 ± 299 nm. A variety of fiber diameters was also observed by Song et al. [29]. From the figure, it can be observed that only a small number of beads appear when the liquid supply ratio is 1:3 and 1:2. However, when the liquid supply ratio is 1:1, a large number of beads appear, and the nanofibers are disorderly and uneven, this may be due to the fact that the shell solution could not completely cover the core solution, resulting in the disorder of Taylor cone, and the disorderly and uneven electrospinning. It is concluded that the electrospinning effect is better when the liquid supply ratio is 1:3 and 1:2, and 1:2 is the best according to the normal analysis of filament diameter. Fig. 4(h) is the energy spectrum analysis diagram of the Ag-NPs-loaded membrane, from which it can be seen that Ag-NPs are present and are distributed in the nanofibers, which can preliminarily prove that Ag-NPs are successfully loaded into the membrane.

TEM is the most effective method for observing the core-shell structure, Fig. 4(e–g) shows the TEM images of coaxial electrospun fibers. Furthermore, the core material is denser than the shell material and shows in black, whereas the shell material shows in gray. As shown in the figure, the core CS-PEO-Ag-NPs was completely encapsulated by PCL, the core-shell structure of nanofibers were well formed. Additionally, the diameter difference between the core and shell under the three core-shell flow rates is measured as 29.36 nm, 84.22 nm, 11.74 nm. The rate of 1:2 was chosen in order to achieve the coverage of the shell, so that the Ag-NPs would be better coated, and membrane can achieve the effect of slow release.

3.2. Infrared spectral analysis

Fig. 5(a) shows the infrared spectra of the sample membrane without Ag-NPs, PCL, CS and PEO. The stretching vibration peak of PCL was at 1727 cm^{-1}. 1655 cm^{-1} and 1650 cm^{-1} was the amide vibration peak of CS and PEO. These three peaks are the unique peaks of the above three materials [30,31]. In the sample membrane, there was a characteristic peak corresponding to PCL at 1729 cm^{-1}, which proved the existence of PCL. The characteristic peaks corresponding to CS and PEO were found
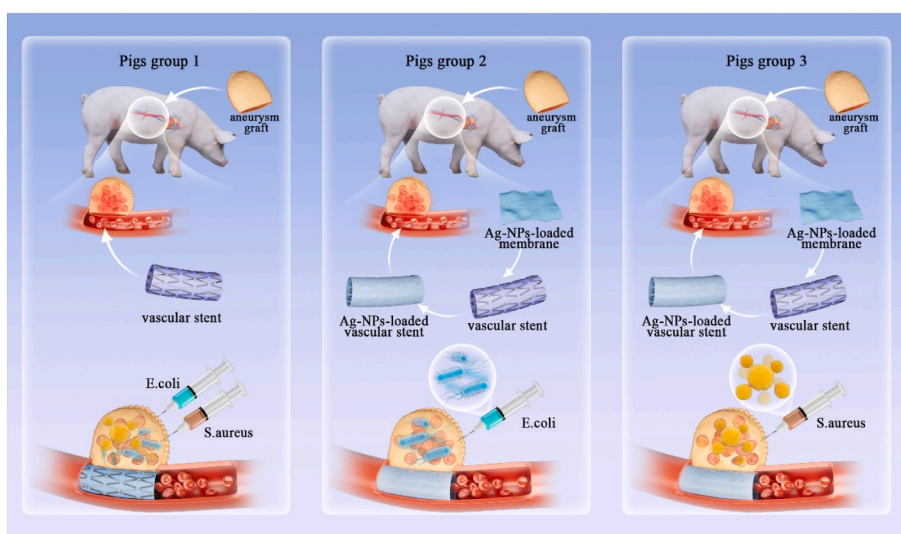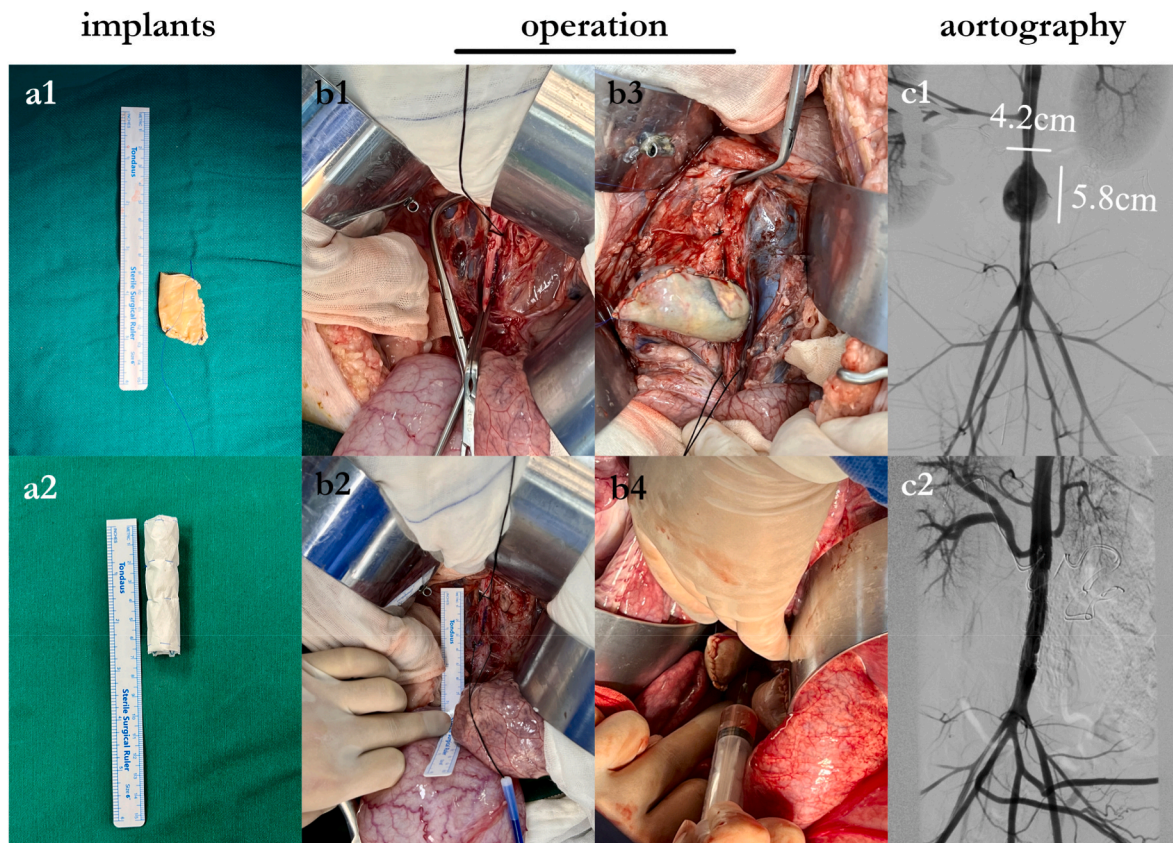

Fig. 2. The flow chart of the operation on the white pigs. First, the aneurysm graft was sutured at the abdominal aorta of pigs; Then vascular stent was implanted into the aneurysm of each pig; Finally, the bacterial solution (*E. coli* and *S. aureus*) was injected into the aneurysm.

implants   operation   aortography

Fig. 3. In vivo experimental records: (a1) Pocket-shaped abdominal aortic aneurysm made of bovine pericardium. (a2) Bare metal vascular stent. (b1-b4) Scenarios of an abdominal aortic aneurysm being implanted. (c1-c2) Abdominal aortography before and after endovascular repairing.

at 1598 cm^{-1}. This conclusion proved the existence of CS and PEO. Fig. 5 (b) shows the infrared spectra of sample membranes with and without Ag-NPs. The infrared spectra of the two sample membranes were roughly the same, only in the range of 1359-1181 cm^{-1}. The characteristic peak intensity of the membrane with Ag-NPs was slightly strengthened. The attenuation of the vibration absorption peak of –OH may be caused by the addition of Ag-NPs. In addition, there was a small characteristic peak of Ag-NPs at 2350 cm^{-1}; these results suggested that Ag-NPs may be physically trapped in the core layer of nanofibers [32].

3.3. Mechanical properties

Fig. 5(c) and Table .2 shows the tensile test diagrams of PCL, CS-PEO/PCL and CS-PEO-Ag-NPs/PCL. It can be seen from the experimental results that the tensile strength and elastic modulus of PCL and CS-PEO/PCL were found as 3.057 ± 0.193 MPa,6.281 ± 0.862 MPa and 1.967 ± 0.071 MPa,5.90 ± 0.727 MPa. When compared to the pure PCL electrospun membrane, the addition of CS and PEO, which have relatively poor mechanical properties, resulted in a decrease in the tensile strength of the coaxial electrospun membrane. However, the elastic modulus remained the same, indicating that the rigidity of the membrane was maintained, making it less susceptible to deformation. After the addition of Ag-NPs, the tensile strength of CS-PEO-Ag-NPs/PCL was 2.108 ± 0.158 MPa, which was slightly improved, it is speculated that the ionic interaction between positively charged silver atoms and partially negatively charged carbonyl groups of PCL leads to higher intermolecular bonding between polymer chains. Therefore, with the addition of Ag-NPs, the membrane obtains better strength and lower elongation at break [33].

As shown in Fig. 5(d), the water contact angle of CS-PEO/PCL membrane is $71.98 \pm 2.545°$, which is much better than that of pure PCL membrane with water contact angle of $117.91 \pm 3.074°$.

Furthermore, the addition of Ag-NPs did not affect the hydrophilicity of the membrane, the water contact angle is only slightly different after the addition. The water contact angle of the Ag-NPs-loaded membranes was about $70.87 \pm 3.928°$, showing neither too hydrophobic nor too hydrophilic. This moderate hydrophilicity is conducive to cell adhesion and growth. The Ag-NPs-loaded membrane remained integrated after irradiation sterilization, sewn onto the stent-graft and resheathed into a 20F delivery system.

3.4. Antibacterial performance

The antibacterial activity of the Ag-NPs-loaded membrane was determined against Gram-negative *Escherichia coli* and Gram-positive *Staphylococcus aureus*, and these two are representatives of positive and negative bacteria [34]. As shown in Fig. 6(a), when the concentration of Ag-NPs was 1 wt%, the antibacterial effect on *E. coli* was not obvious, while the concentration increased to 2 wt%, 3 wt%, the antibacterial is obvious. Fig. 6(b) shows that when the concentration of Ag-NPs was 1 wt%,2 wt%, the antibacterial effect on *S. aureus* was just a little. However, when the concentration was increased to 3 wt%, the inhibition circle was more obvious than that of 1 wt% and 2 wt%. There was no significant change in these inhibition circles until 120 h. Due to the bacteriostatic mechanism of Ag-NPs, Ag-NPs do not disappear after killing the bacteria. Therefore, it can be inferred that the Ag-NPs-loaded membrane has a long-term antibacterial effect.

3.5. Ag-NPs release performance

The release rate of Ag-NPs was studied by measuring the absorbance of Ag-NPs in liquid at a time point by spectrophotometer, converting it into concentration by the standard curve of Ag-NPs, and then drawing the release curve as shown in Fig. 7(a). As can be seen from the figure, all
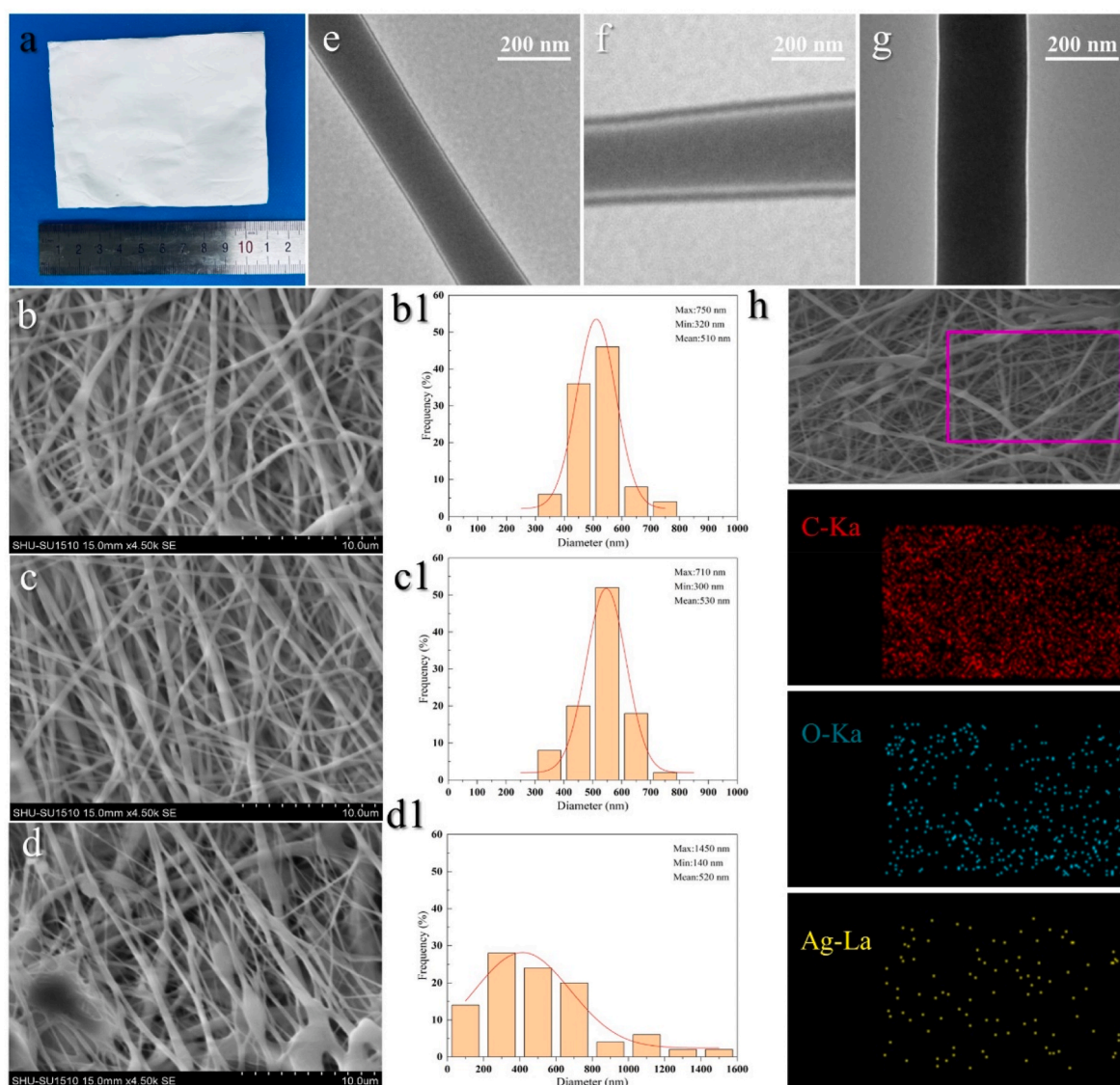
Fig. 4. Physical characterization of Ag-NPs-loaded membrane. (b-d, b1-d1) SEM images of Ag-NPs-loaded membranes and normal statistical graph of diameter distribution, the core-shell liquid supply ratios are (b) 1:3, (c) 1:2, (d) 1:1; The scalar bar is 10 μm. (e–g) TEM images of coaxial electrospun fibers, the core-shell liquid supply ratios are (e) 1:3, (f) 1:2 (g) 1:1; The scalar bar is 200 nm; (h) Energy spectrum analysis diagram.

three membranes showed sudden release in the first 24 h, in the case of Ag-NPs-loaded membranes, it may be that some fibers are not fully coated with Ag-NPs, causing Ag-NPs to be present on the surface and resulting in sudden release. However, after 24 h, the release rate of coaxial electrospun membranes obviously slowed down, and the release rate of the uniaxial electrospun membrane remained fast, and there was a significant difference in the release rate between them. The results show that the drug release rate could be controlled by coaxial electrospinning. With this function, membrane can prevent Ag-NPs sudden release, the sudden release of Ag-NPs dose is large, produce toxic side effects, failed to play a good therapeutic effect [35].The membranes prepared in this experiment have the function of drug-sustained release, and can be released for a long time, so as to achieve a long-term antibacterial effect.

3.6. Cytotoxicity and cell adhesion of Ag-NPs-loaded membranes

In order to observe the cell morphology and the distribution of live and dead cells on the membranes after 1, 3 and 5 days of culture, HUVECs was tested by live-dead staining, and results are shown in Fig. 7

(b–g, b1-g1). In the 1 d, the number of cells on the two groups of membrane was balanced. However, up to 3 d and 5 d, cells on the Ag-NPs-loaded membrane proliferated more compared to the pure PCL membrane, because the Ag-NPs-loaded membrane has better hydrophilicity and is more conducive to cell adhesion. But there were a little more dead cells, which was within the normal range, cells death may be due to the cells gathered too densely, leading to the death of individual cells due to hypoxia. The results prove that the Ag-NPs-loaded membrane was not cytotoxic and was beneficial to cell adhesion.

Fig. 7(h) shows the absorbance of each group, which is used to analyze cell survival rate. After 1, 3 and 5 days of culture, the OD value of each group gradually increased, and cell proliferation trend was basically the same. According to the significance difference analysis, there was a statistically significant difference between three groups only on the first day. By 3 days of culture, the Ag-NPs-loaded membrane and PCL membrane both had higher cell survival rate than control group, there was no statistically significant difference between them. Until 5 days of culture, the cell survival rate of Ag-NPs-loaded membrane and PCL membrane still higher than control group, and there was no statistically significant difference between them. This shows that Ag-NPs-
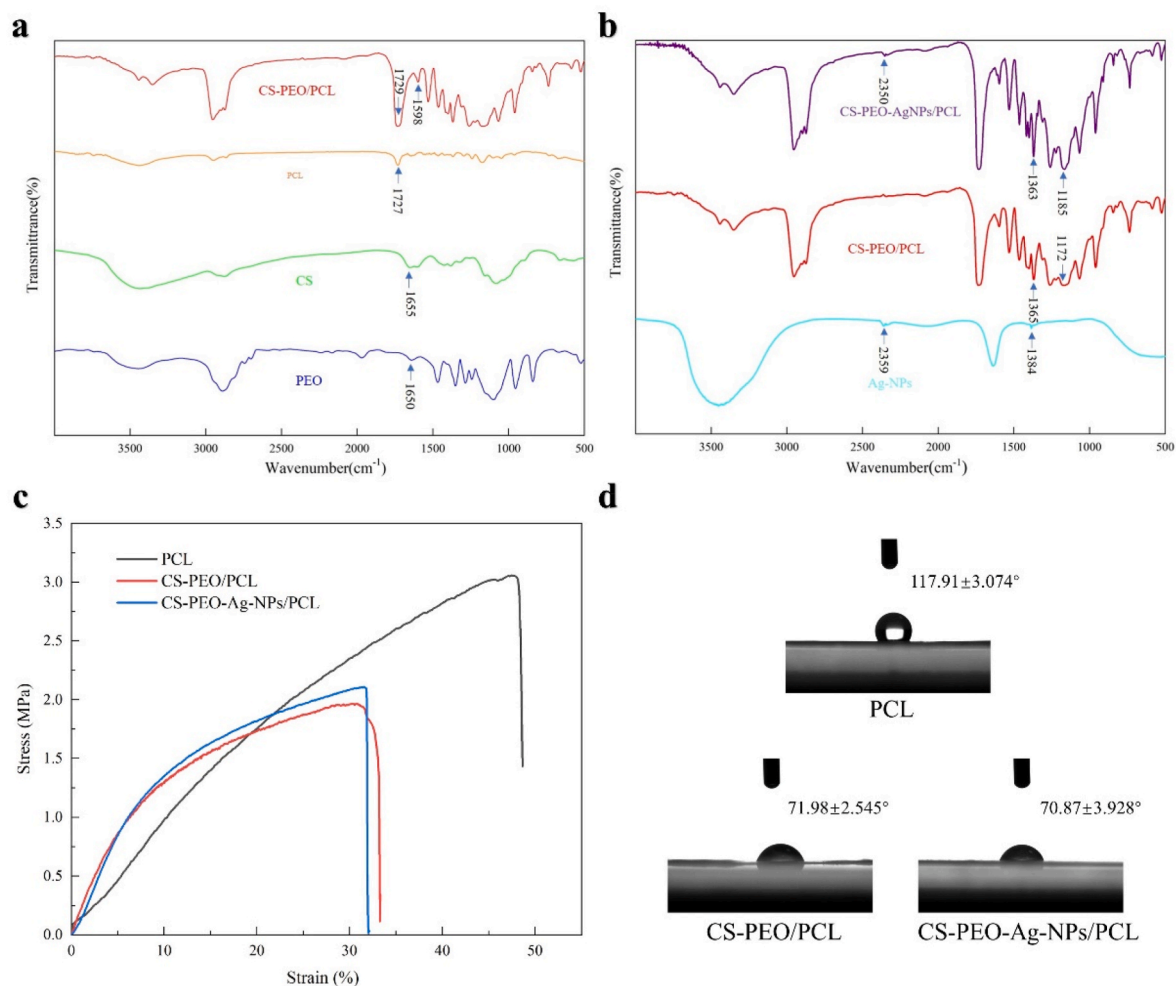
Fig. 5. Characterization of membranes: (a) FTIR spectra of PCL, CS, PEO and membrane CS-PEO/PCL; (b) FTIR spectra of Ag-NPs and membrane CS-PEO-Ag-NPs/PCL, membrane CS-PEO/PCL. (c) Tensile strain curve of membranes: PCL; CS-PEO/PCL; CS-PEO-Ag-NPs/PCL; (d) Water contact Angle of membranes: PCL; CS-PEO/PCL; CS-PEO-Ag-NPs/PCL.

Table 2
Tensile properties of the electrospun fibers membranes.

Samples	Tensile Strength (MPa)	Strain at break (%)	Elastic Modulus (MPa)
PCL	3.057 ± 0.193	48.627 ± 8.066	6.281 ± 0.862
CS-PEO/PCL	1.967 ± 0.071	33.321 ± 5.112	5.90 ± 0.727
CS-PEO-Ag-NPs/ PCL	2.108 ± 0.158	33.142 ± 4.618	6.361 ± 1.387

loaded membrane was nontoxic, and the addition of appropriate amounts of Ag-NPs did not inhibit cell survival and proliferation.

3.7. In vivo experiments pathology and results

All experimental pigs survived through 1 month after surgery. As shown in Fig. 8(a1-c1, a2-c2), ultrasonography showed patency of the abdominal aorta, renal artery and iliac artery. Abdominal aortography showed dimensions of abdominal aortic aneurysm sac (a1: 4.6*3.2 cm, b1: 6.0*4.0 cm, c1: 5.8*4.2 cm). No dislocation of the stents was evidenced.

General observation from Fig. 8(a3-c4, a4-c4) found that there was fluid part in the abdominal aortic aneurysm sac, while most part was filled with organized thrombus. General observation found that there were significantly more organized thrombus and less fluid in the aneurysm sacs of group 2 and 3, compared with group 1.

As shown in Fig. 9(a1-c1, a2-c2), HE staining showed that there was no obvious inflammatory cell infiltration in aneurysm sac of group 1. No significant inflammatory response was observed, and *E. coli* and *S. aureus* were colonized well along the outer surface of the stent-graft with specific value (a1: 3.7 %, a2: 3.5 %). The inflammatory cell infiltration in aneurysm sac of group 2,3 was significantly more than that of group 1. The inflammatory cell infiltration in aneurysm sac of group 2 was even more than that of group 3. The outer surfaces of stent-graft in group 2 and 3 were covered by neoplastic endothelium composed predominantly of fibroblasts. And the nearby aortic wall was also infiltrated by inflammatory cells with specific value (b1: 18.1 %, b2: 17.0 %, c1: 12.6 %, c2: 12.4 %). The nearby aortic wall structure was preserved better in group 2 and 3, compared with group 1.

The quantification of bacteria in the aneurysm sacs was assessed by Gram staining. As shown in Fig. 9(a3-c3, a4-c4), In the aneurysm wall and surrounding tissues of Pigs group 1, massive colonization of *E. coli* was evidenced with specific value (a3: 37.2 %, a4: 37.1 %). In group 2, *E. coli* was negative in the aneurysm sac, nearby aortic wall and surrounding tissues with specific value (b3: 6.5 %, b4: 6.0 %). In group 3, *S. aureus* was also negative in the aneurysm sac, nearby aortic wall and surrounding tissues with specific value (c3: 4.6 %, c4: 4.1 %).
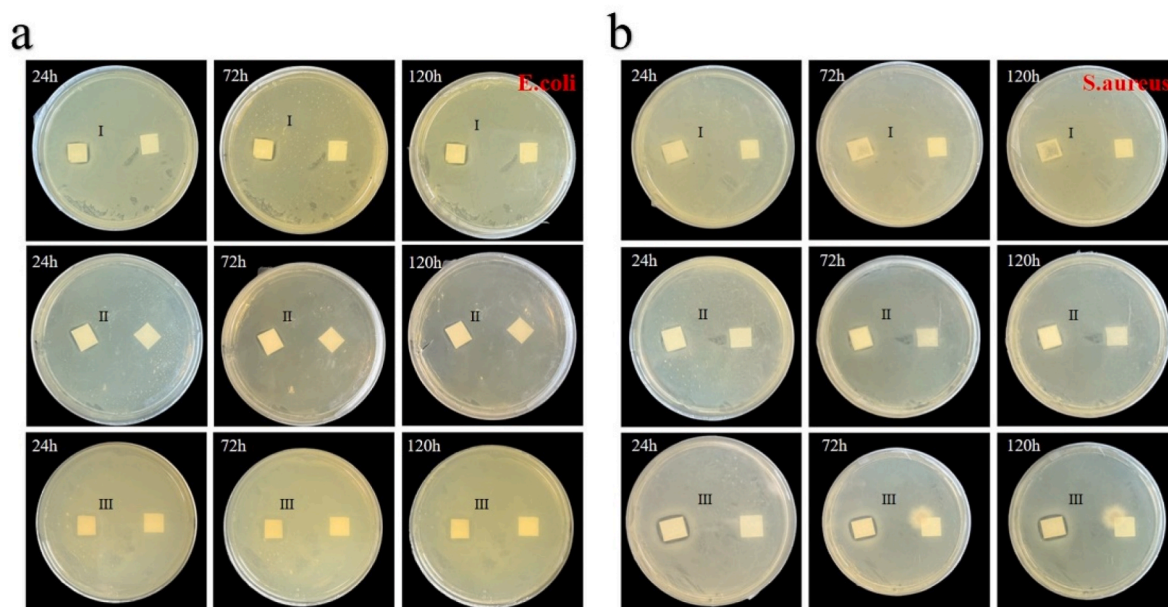
Fig. 6. Antibacterial activity of membrane depicted by the diffusion results at different Ag-NPs concentrations of (I)1 wt%(II)2 wt%(III)3 wt% against: (a) *E. coli*; (b) *S. aureus*.

4. Discussions

Stent-graft infection following endovascular repair of aortic diseases poses a challenging clinical problem, and the prognosis could be poor and lethal. There are two main scenarios in which stent-graft infection can occur. Firstly, the emergent endovascular repair of a rupture or pending-rupture mycotic aortic aneurysm. Stent-grafts are infected after implantation into the infection lesions. Staged drainage and long-term use of systemic antibiotics have been reported to be effective to control the stent-graft infection [36]. If the infection cannot be controlled, open surgery conversion is recommended to remove the stent graft and the whole infected lesion even though the procedure is complicated [37]. Secondly, there were studies reported that non-infected aortic diseases were treated by endovascular procedure, but the stent-graft got infected during the perioperative period or months even years after procedure [38]. The prognosis in these cases may be even worse, as the infections can be caused by antibiotic-resistant bacteria.

So, if we can develop an antimicrobial endograft, it may be applied in two scenarios in clinic. First, in mycotic aortic aneurysms, if local antimicrobial shield can be established by preventing the infection of endograft with Ag-NPs-loaded membranes, there would be a chance to conduct staged transcutaneous drainage and systemic antibiotics. And in this way, the chance of endovascular repair of mycotic aortic aneurysms might be improved. Second, for non-infected aortic diseases, some patients are at high risk of developing endograft infection, such as the patients with diabetes, Immunodeficiency diseases, long-term use of glucocorticoids, poor fitness or innutrition et al. They would suffer from endograft infection at any time after the procedure or in long-term follow-up [28]. The long-lasting of Ag-NPs is required to prevent the stent-graft infection. If Ag-NPs could exist in the affected area for a long time, it might prevent endograft infection in selected cases.

In this study, a drug-loaded vascular membrane with antibacterial function and sustained drug release function, the Ag-NPs-loaded membrane, was prepared by coaxial electrospinning technology. Due to the drug-loaded membrane prepared by blend electrospinning can only attach the drugs to the surface of fibers, this leads to drug quickly lost after blood erosion after implantation into the body, and the long-term antibacterial effect cannot be achieved. Coaxial electrospinning is a kind of electrospinning technique of preparing fibers with a core-shell structure [39]. Compared with traditional electrospinning, coaxial electrospinning can encapsulate drug in the core layer of fibers to avoid the rapid loss of drug due to blood erosion and has better performance in drug loading and slow release [40]. This technology has been widely used in the biomedical field [41].

In the coaxial electrospinning process, the liquid supply ratio of core-shell solution directly affects the formation quality of nanofibers and the forming of core-shell structure. We set three groups of parameters, when the liquid supply ratio is 1:2, the distribution diameter of nanofibers in the membrane is the most uniform, and the core-shell structure is well formed, and the drug is well wrapped in the inner layer. Therefore, we chose the liquid supply ratio of 1:2 as the parameter for membrane preparation. In addition, the membrane covered on stent in human blood vessels would be subjected to pressure from blood flow; therefore, the mechanical properties of membranes are essential for tissue engineering applications [42]. With the addition of CS and PEO, the tensile strength of the membrane prepared by coaxial electrospinning reached 2.108 ± 0.158 MPa. Although the tensile strength of Ag-NPs-loaded membrane is lower than that of PCL membrane prepared by uniaxial electrospinning, Ag-NPs-loaded membrane can still meet the mechanical performance requirements of human arterial blood vessels.

Hydrophilicity is an important index to evaluate the potential biological properties of vascular stent membranes. The membrane with better surface hydrophilicity is conducive to cell adhesion and proliferation, but the hydrophilicity will also affect cell migration. Therefore, the surface hydrophilicity of the membrane should not be too good. Due to the good hydrophilicity of CS and PEO, their addition can improve the hydrophilicity of the membrane. The water contact angle of the Ag-NPs-loaded membranes was about $70.87 \pm 3.928°$, showing good hydrophilicity, but not too hydrophilic. The effectiveness of cell inoculation is one of the important factors to evaluate the biocompatibility of membrane. Cell adhesion test showed that Ag-NPs-loaded membrane was more conducive to cell adhesion and proliferation than PCL membrane. Meanwhile, nanoparticles that show antimicrobial activity, including Ag-NPs, especially in the case of high concentration will be toxic to human cell, and even harmful to human health [43]. The cytotoxicity of the Ag-NPs-loaded membrane was detected by CCK-8. The results showed that the addition of Ag-NPs had little toxicity to HUVECs, the Ag-NPs-loaded membrane showed good biocompatibility and safety.

Maintaining the long-term drug release function and long-term bacteriostatic effect of the membrane is an urgent problem to be
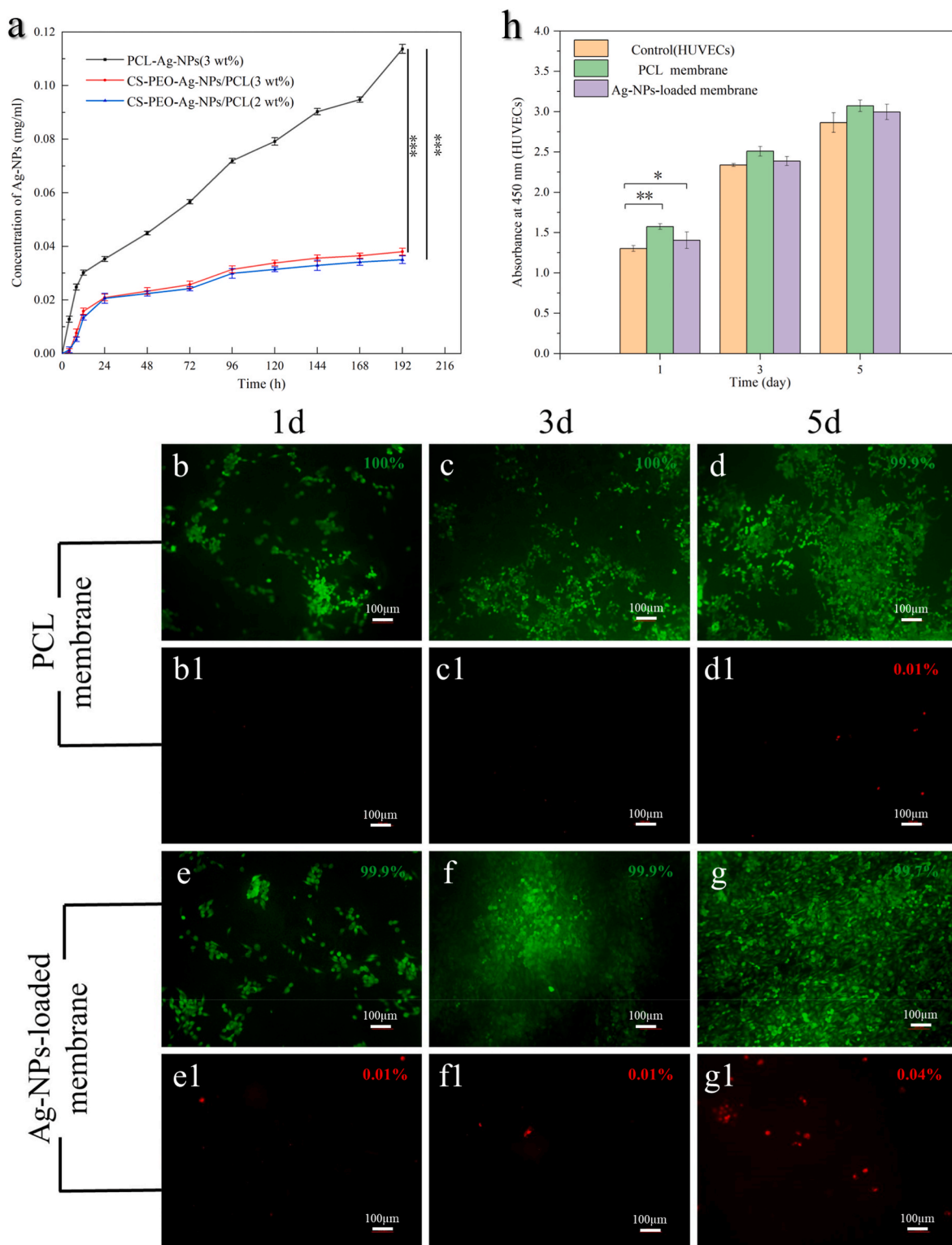
Fig. 7. The release rate curve diagram, the live/dead fluorescence images and CCK-8 assays of HUVECs on the membranes were observed after 1,3 and 5 days of culture. (a)Ag-NPs release rate curve of pure PCL and Ag-NPs-loaded membranes(***$p < 0.001$, n = 5); (b–d) images of living cells in the PCL membrane. (b1-d1) Images of dead cells in the pure PCL membrane. (e–g) Images of living cells in the Ag-NPs-loaded membrane. (e1-g1) Images of dead cells in the Ag-NPs-loaded membrane. (h) Cell proliferation on different membranes after culturing for 1,3 and 5 days: PCL membrane, Ag-NPs-loaded membrane and Control(HUVECs) (*$p < 0.05$,n = 3; **$p < 0.01$, n = 3).

solved in tissue engineering. At present, amoxicillin, vancomycin and cephalosporin are commonly used as antibacterial drugs. In this study, Ag-NPs were chosen as the drug loaded on the membrane. Studies had found that Ag-NPs produce antibacterial effects by binding to and

penetrating the bacterial cell wall, after entering the cell wall, Ag-NPs will cause structural changes, disrupt the biochemical processes of DNA, cell enzymes and respiratory systems, and lead to bacterial death [44,45]. After killing bacteria, Ag-NPs will be free from bacteria to
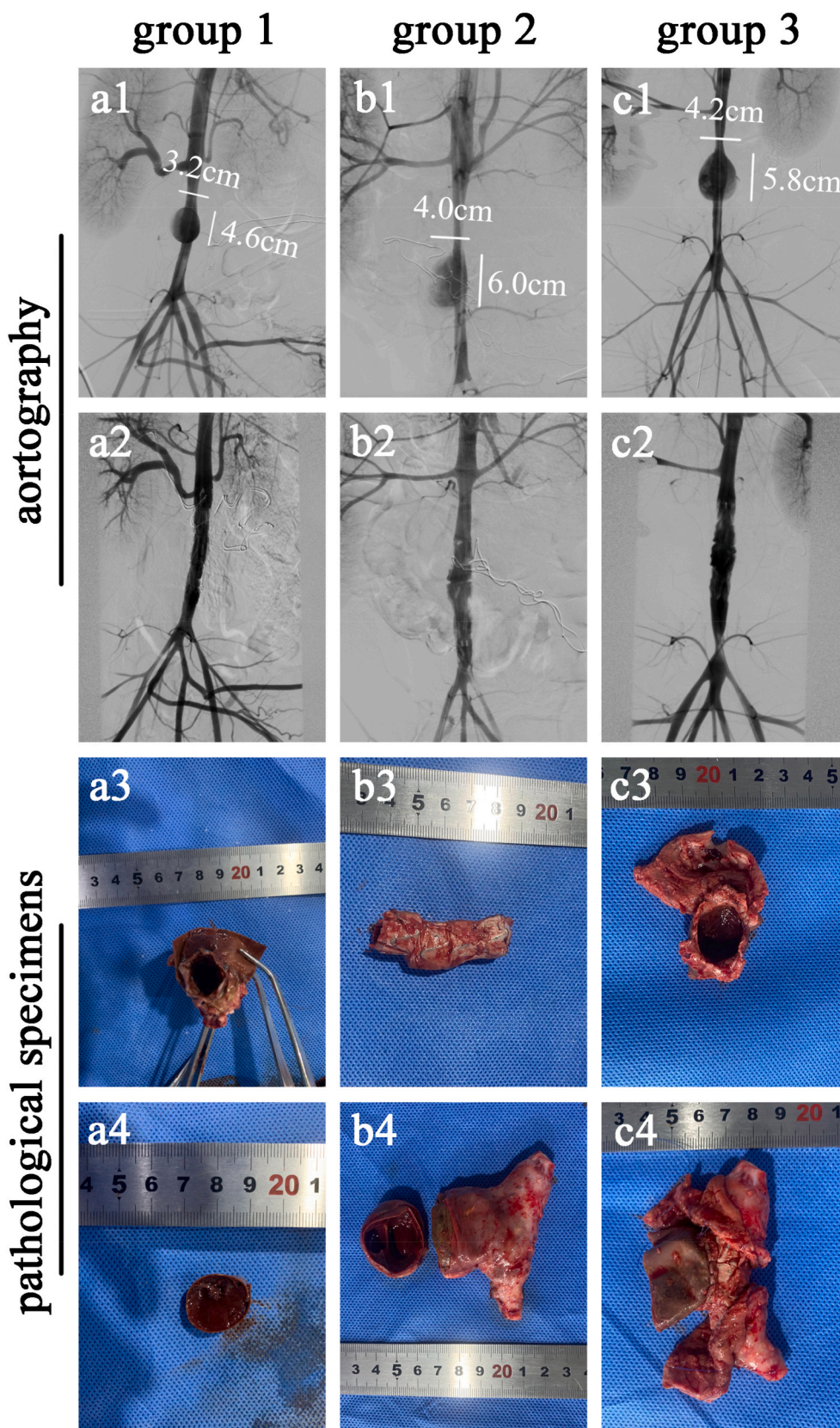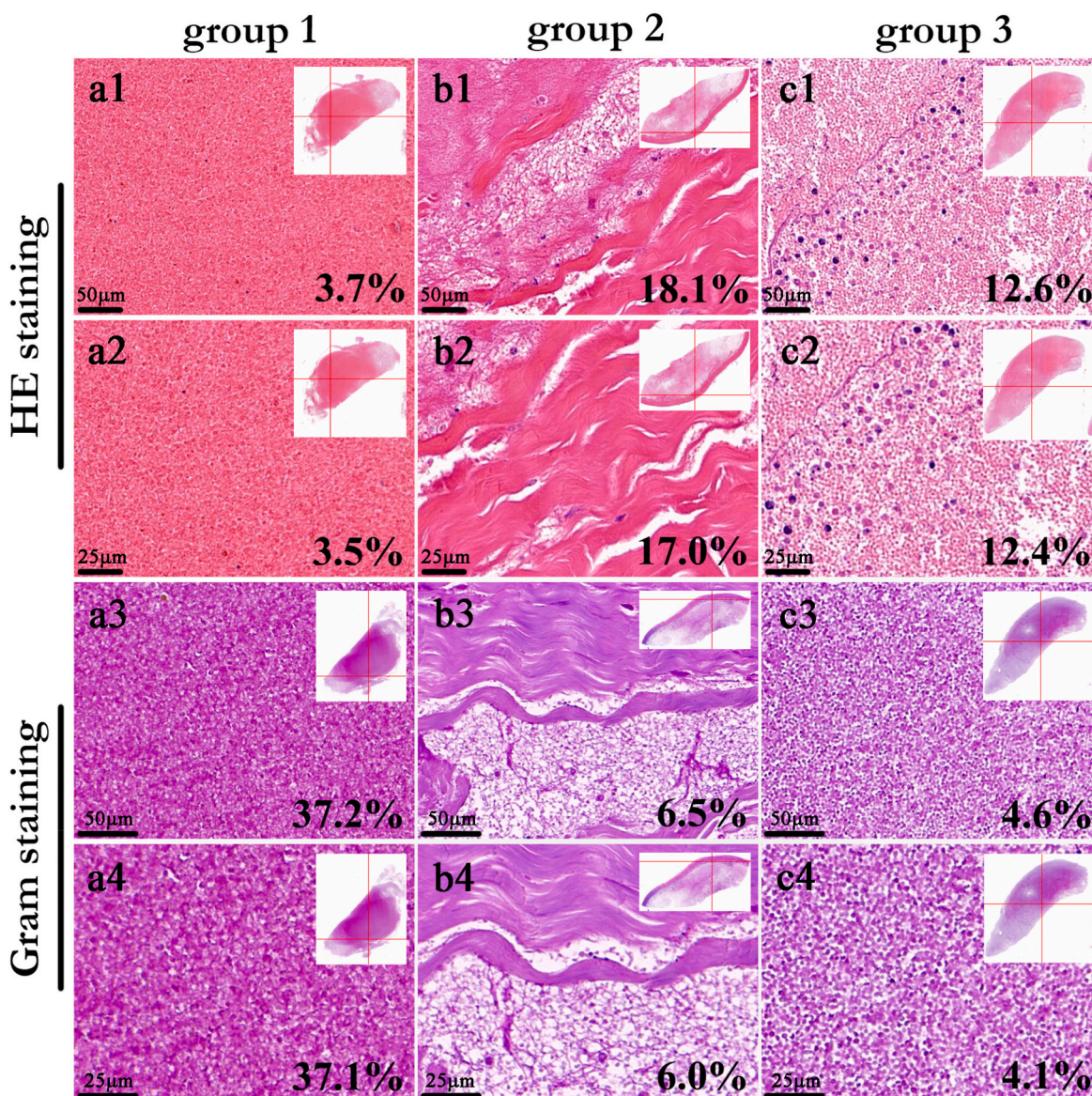
Fig. 8. Abdominal Aortography of pigs and endograft samples (a1-c1, a2-c2) Abdominal aortography before and after endovascular repairing in the manner of "Flow speed: 15 ml/s, Volume: 25 ml, Pressure: 800PSI. Contrast: Iodixanol (GE Healthcare, USA)". (a3-c3, a4-c4) pathological specimens and implanted stents collected for general pathology.

Fig. 9. Microscopic pathological HE staining and Gram staining: (a1-a2) Only blood cells in the aneurysm cavity of Pigs group 1. (a3-a4) In Pigs group 1, massive aggregations of *E. coli* were expressed as saffron color with assistance of staining. (b1-b2) Aneurysm wall of Pigs group 2 was mechanized and covered by neoplastic intima dominated by fibroblasts. (b3-b4) *E. coli* is hardly visible in aneurysm wall and surrounding tissues of Pigs group 2. (c1-c2) Plenty of neutrophils and macrophages infiltrate the aneurysm wall of Pigs group 3. (c3-c4) *S. aureus* is difficult to detect in the view of Pigs group 3 due to Gram staining characteristics and there is no *E. coli*. (For interpretation of the references to color in this figure legend, the reader is referred to the Web version of this article.)

continue to produce antibacterial effects. When testing its antibacterial properties, we selected *E. coli* and *S. aureus* as the representatives of negative/positive bacteria. The results showed that when the addition of Ag-NPs reached 3 wt%, the antibacterial effect of the membrane was obvious, and the inhibition circle remained unchanged within 120 h. Due to the lack of longer observation, it could only be preliminarily inferred that the Ag-NPs-loaded membrane has long-term antibacterial function, which needs further verification in the future. In the release test of Ag-NPs, the release rate of Ag-NPs-loaded membrane prepared by coaxial electrospinning was much slower than that of the uniaxial electrospun membrane. The sustained drug release function of Ag-NPs-loaded membrane is attributed to the coaxial electrospinning, which encapsulates Ag-NPs in the inner layer of nanofibers. The sudden release phenomenon in the first 24 h may be due to the small amount of Ag-NPs were attached to the surface of nanofibers, which were quickly released into the PBS after washing [46,47], and the remaining Ag-NPs wrapped by nanofibers were slowly released [48]. However, the release

rate of Ag-NPs was only assessed in vitro using Pbs solution, and the detection cycle was limited only to 196 h. Further research is necessary to confirm the long-term sustained release function of the Ag-NPs-loaded membrane after implantation in vivo.

Due to the porcine aorta has similarities with the human abdominal aorta in terms of morphology, physiology, and branch vessel distribution [49], it is appropriate model for studying abdominal aortic aneurysms and evaluating the efficacy and safety of metal vascular stents with Ag-NPs-loaded membranes [50]. Results of HE staining of porcine aneurysm grafts showed that the pig implanted with stent covered with Ag-NPs-loaded membrane had a significant higher rate of organized thrombus in aneurysm sac and inflammatory infiltration. Furthermore, Gram staining results showed that bacteria were almost invisible on the aneurysm wall, nearby aortic wall, and surrounding tissues in pigs with Ag-NPs-loaded membrane. On the contrary, significant bacterial colonization was observed in the pigs with conventional stent-graft. These findings revealed the effectiveness of the antibacterial effects of the

Ag-NPs-loaded membrane. Ag-NPs-loaded membrane successfully released Ag-NPs into the aneurysm sac and inhibited the bacterial colonization. Besides, optimal biocompatibility of the Ag-NPs-loaded membranes was also evidenced by the integrated structure of the aortic wall where the Ag-NPs-loaded membrane was landed on.

4.1. Limitation

The mechanical properties and thickness of the membrane should be further optimized, so that it not only can cover the existing covered stent, but also can realize the exclusion function of the artificial vascular membrane of the current stent-graft. Then it can be directly combined with nitinol stent skeleton. In this way, the profile of delivery system of this antibacterial stent-graft could be significantly reduced, so as to realize the delivery through peripheral arteries such as femoral artery. Moreover, the release behavior of Ag-NPs on the membrane can be optimized to make it controllable, such as PH, temperature or electromagnetic response, which would fulfill different antibacterial time-histories requirements in clinic.

5. Conclusion

Aortic stent-graft loaded with Ag-NPs membrane constructed by coaxial electrospinning technology, had the slow-release function of Ag-NPs, so as to exert long-term antibacterial function. The Ag-NPs-loaded membrane were composed of PCL as the shell, CS and PEO as the core, and Ag-NPs incorporated into the core. In-vitro and in-vivo experiments demonstrated the good biocompatibility and inhibition function of the Ag-NPs-loaded membrane on *E. coli* and *S. aureus*. It might provide a promising method to fight the mycotic aortic pathologies.

CRediT authorship contribution statement

Qingxi Hu: Conceptualization, Data curation, Writing - original draft, Writing - review & editing. **Zhenwei Huang:** Conceptualization, Investigation, Writing - original draft, Writing - review & editing. **Haiguang Zhang:** Conceptualization, Data curation, Funding acquisition, Investigation, Project administration, Resources, Writing - review & editing. **Pengcheng Ma:** Conceptualization, Investigation, Supervision, Writing - original draft, Writing - review & editing. **Rui Feng:** Conceptualization, Data curation, Methodology, Resources, Writing - review & editing. **Jiaxuan Feng:** Conceptualization, Data curation, Formal analysis, Investigation, Resources, Validation, Writing - original draft, Writing - review & editing.

Declaration of competing interest

The authors declared no potential conflict of interest with respect to the research, author-ship and publication of this article.

Data availability

Data will be made available on request.

Acknowledgements

Abbreviations

PTFE	Polytetrafluoroethylene
PET	Polyethylene terephthalate
Ag-NPs	Silver nanoparticles
PCL	Polycaprolactone
CS	Chitosan
PEO	Polyethylene oxide
DCM	Dichloromethane
DMF	N, N-Dimethylformamide
Hac	Acetic acid
E. coli	Escherichia coli
S. aureus	Staphylococcus aureus
PLD	Pulsed laser deposition
LBL	Layer-by-layer
PLA	Polyactic acid
SEM	Scanning electron microscope
TEM	Transmission electron microscopy

References

[1] S. Lessim, S. Oughlis, J.J. Lataillade, V. Migonney, S. Changotade, D. Lutomski, F. Poirier, Protein selective adsorption properties of a polyethylene terephtalate artificial ligament grafted with poly(sodium styrene sulfonate) (polyNaSS): correlation with physicochemical parameters of proteins, Biomed. Mat. 10 (6) (2015) 10, https://doi.org/10.1088/1748-6041/10/6/065021.

[2] Y. Roina, F. Auber, D. Hocquet, G. Herlem, ePTFE-based biomedical devices: an overview of surgical efficiency, J. Biomed. Mat. Res Part B-Appl. Biomat. 110 (2) (2022) 302–320, https://doi.org/10.1002/jbm.b.34928.

[3] C. Ergene, K. Yasuhara, E.F. Palermo, Biomimetic antimicrobial polymers: recent advances in molecular design, Polym. Chem. 9 (18) (2018) 2407–2427, https://doi.org/10.1039/c8py00012c.

[4] S.Q. Li, S.J. Dong, W.G. Xu, S.C. Tu, L.S. Yan, C.W. Zhao, J.X. Ding, X.S. Chen, Antibacterial hydrogels, Adv. Sci. 5 (5) (2018) 17, https://doi.org/10.1002/advs.201700527.

[5] S.J. Lam, E.H.H. Wong, C. Boyer, G.G. Qiao, Antimicrobial polymeric nanoparticles, Prog. Polym. Sci. 76 (2018) 40–64, https://doi.org/10.1016/j.progpolymsci.2017.07.007.

[6] K. Gavali, K. Mani, M. Furebring, K.W. Olsson, D. Lindstrom, K. Sorelius, B. Sigvant, K.D. Gidlund, G. Torstensson, M. Andersson, C. Forssell, H. Astrand, T. Lundstrom, S. Khan, B. Sonesson, O. Stackelberg, P. Gillgren, J. Isaksson, B. Kragsterman, T. Horer, M. Sadeghi, A. Wanhainen, Outcome of radical surgical treatment of abdominal aortic graft and endograft infections comparing extra-anatomic bypass with in situ reconstruction: a Nationwide Multicentre Study, Eur. J. Vasc. Endovasc. Surg. 62 (6) (2021) 918–926, https://doi.org/10.1016/j.ejvs.2021.09.033.

[7] J. Li, D. Zhai, F. Lv, Q. Yu, H. Ma, J. Yin, Z. Yi, M. Liu, J. Chang, C. Wu, Preparation of copper-containing bioactive glass/eggshell membrane nanocomposites for improving angiogenesis, antibacterial activity and wound healing, Acta Biomater. 36 (2016) 254–266, https://doi.org/10.1016/j.actbio.2016.03.011.

[8] Y. Yu, R. Cui, X. Wang, H. Yang, H. Li, Preparation of multifunctional poly(l-lactic acid) film using heparin-mimetic polysaccharide multilayers: hemocompatibility, cytotoxicity, antibacterial and drug loading/releasing properties, Int. J. Biol. Macromol. 155 (2020) 14–26, https://doi.org/10.1016/j.ijbiomac.2020.03.180.

[9] H.H. Huang, C.L. He, H.S. Wang, X.M. Mo, Preparation of core-shell biodegradable microfibers for long-term drug delivery, J. Biomed. Mater. Res., Part A 90A (4) (2009) 1243–1251, https://doi.org/10.1002/jbm.a.32543.

[10] P.P. Rade, P.S. Giram, A.A. Shitole, N. Sharma, B. Garnaik, Physicochemical and in vitro antibacterial evaluation of metronidazole loaded eudragit S-100 nanofibrous mats for the intestinal drug delivery, Adv. Fiber Mater. 4 (1) (2022) 76–88, https://doi.org/10.1007/s42765-021-00090-y.

[11] A.C. de Luca, J.S. Stevens, S.L. Schroeder, J.B. Guilbaud, A. Saiani, S. Downes, G. Terenghi, Immobilization of cell-binding peptides on poly-epsilon-caprolactone film surface to biomimic the peripheral nervous system, J. Biomed. Mater. Res. 101 (2) (2013) 491–501, https://doi.org/10.1002/jbm.a.34345.

[12] Zhang, Y.; Xu, K.; Zhi, D. K.; Qian, M. Y.; Liu, K. Z.; Shuai, Q. Z.; Qin, Z.; Xie, J. H.; Wang, K.; Yang, J., Improving Vascular Regeneration Performance of Electrospun Poly(epsilon-Caprolactone) Vascular Grafts via Synergistic Functionalization with VE-Cadherin/VEGF. Adv. Fiber Mater, 18.http://doi.org/10.1007/s42765-022-00213-z. .

[13] O. Ozkan, H. Turkoglu Sasmazel, Effects of nozzle type atmospheric dry air plasma on L929 fibroblast cells hybrid poly (epsilon-caprolactone)/chitosan/poly (epsilon-caprolactone) scaffolds interactions, J. Biosci. Bioeng. 122 (2) (2016) 232–239, https://doi.org/10.1016/j.jbiosc.2016.01.004.

[14] A. Cooper, N. Bhattarai, M. Zhang, Fabrication and cellular compatibility of aligned chitosan–PCL fibers for nerve tissue regeneration, Carbohydr. Polym. 85 (1) (2011) 149–156, https://doi.org/10.1016/j.carbpol.2011.02.008.

[15] R.A.A. Muzzarelli, Chitosan composites with inorganics, morphogenetic proteins and stem cells, for bone regeneration, Carbohydr. Polym. 83 (4) (2011) 1433–1445, https://doi.org/10.1016/j.carbpol.2010.10.044.

[16] K.T. Shalumon, K.H. Anulekha, C.M. Girish, R. Prasanth, S.V. Nair, R. Jayakumar, Single step electrospinning of chitosan/poly(caprolactone) nanofibers using formic acid/acetone solvent mixture, Carbohydr. Polym. 80 (2) (2010) 413–419, https://doi.org/10.1016/j.carbpol.2009.11.039.

[17] B. Duan, C.H. Dong, X.Y. Yuan, K.D. Yao, Electrospinning of chitosan solutions in acetic acid with poly(ethylene oxide), J. Biomater. Sci. Polym. Ed. 15 (6) (2004) 797–811, https://doi.org/10.1163/156856204774196171.

[18] A. Di Martino, M. Sittinger, M.V. Risbud, Chitosan: a versatile biopolymer for orthopaedic tissue-engineering, Biomaterials 26 (30) (2005) 5983–5990, https://doi.org/10.1016/j.biomaterials.2005.03.016.

[19] T.H. Kim, H.L. Jiang, D. Jere, I.K. Park, M.H. Cho, J.W. Nah, Y.J. Choi, T. Akaike, C.S. Cho, Chemical modification of chitosan as a gene carrier in vitro and in vivo, Prog. Polym. Sci. 32 (7) (2007) 726–753, https://doi.org/10.1016/j.progpolymsci.2007.05.001.

[20] V.R. Sinha, A.K. Singla, S. Wadhawan, R. Kaushik, R. Kumria, K. Bansal, S. Dhawan, Chitosan microspheres as a potential carrier for drugs, Int. J. Pharm. 274 (1–2) (2004) 1–33, https://doi.org/10.1016/j.ijpharm.2003.12.026.

[21] Y. Li, P. Leung, L. Yao, Q.W. Song, E. Newton, Antimicrobial effect of surgical masks coated with nanoparticles, J. Hosp. Infect. 62 (1) (2006) 58–63, https://doi.org/10.1016/j.jhin.2005.04.015.

[22] B. Shan, Y.Z. Cai, J.D. Brooks, H. Corke, Antibacterial properties of Polygonum cuspidatum roots and their major bioactive constituents, Food Chem. 109 (3) (2008) 530–537, https://doi.org/10.1016/j.foodchem.2007.12.064.

[23] X. Chen, H.J. Schluesener, Nanosilver: a nanoproduct in medical application, Toxicol. Lett. 176 (1) (2008) 1–12, https://doi.org/10.1016/j.toxlet.2007.10.004.

[24] S. Akmaz, E.D. Adiguzel, M. Yasar, O. Erguven, The effect of Ag content of the chitosan-silver nanoparticle composite material on the structure and antibacterial activity, Adv. Mater. Sci. Eng. 2013 (2013) 6, https://doi.org/10.1155/2013/690918.

[25] H.L. Jiang, Y.Q. Hu, P.C. Zhao, Y. Li, K.J. Zhu, Modulation of protein release from biodegradable core-shell structured fibers prepared by coaxial electrospinning, J. Biomed. Mater. Res., Part B 79B (1) (2006) 50–57, https://doi.org/10.1002/jbm.b.30510.

[26] I.C. Liao, S.Y. Chew, K.W. Leong, Aligned core-shell nanofibers delivering bioactive proteins, Nanomedicine 1 (4) (2006) 465–471, https://doi.org/10.2217/17435889.1.4.465.

[27] S.H. Liu, Q.X. Hu, Z.P. Shen, S. Krishnan, H.G. Zhang, M. Ramalingam, 3D printing of self-standing and vascular supportive multimaterial hydrogel structures for organ engineering, Biotechnol. Bioeng. 119 (1) (2022) 118–133, https://doi.org/10.1002/bit.27954.

[28] W.R. Wilson, T.C. Bower, M.A. Creager, S. Amin-Hanjani, P.T. O'Gara, P. B. Lockhart, R.O. Darouiche, B. Ramlawi, C.P. Derdeyn, A.F. Bolger, M.E. Levison, K.A. Taubert, R.S. Baltimore, L.M. Baddour, American Heart Association Committee on Rheumatic Fever, E.; Kawasaki Disease of the Council on Cardiovascular Disease in the, Y.; Council on, C.; Stroke, N.; Council on Cardiovascular, R.; Intervention; Council on Cardiovascular, S.; Anesthesia; Council on Peripheral Vascular, D.; Stroke, C., Vascular graft infections, mycotic aneurysms, and endovascular infections: a scientific statement from the American Heart Association, Circulation 134 (20) (2016) e412–e460, https://doi.org/10.1161/CIR.0000000000000457.

[29] W. Song, X. Yu, D.C. Markel, T. Shi, W. Ren, Coaxial PCL/PVA electrospun nanofibers: osseointegration enhancer and controlled drug release device, Biofabrication 5 (3) (2013) 035006, https://doi.org/10.1088/1758-5082/5/3/035006.

[30] L. Ghasemi-Mobarakeh, M.P. Prabhakaran, M. Morshed, M.H. Nasr-Esfahani, S. Ramakrishna, Electrospun poly(epsilon-caprolactone)/gelatin nanofibrous scaffolds for nerve tissue engineering, Biomaterials 29 (34) (2008) 4532–4539, https://doi.org/10.1016/j.biomaterials.2008.08.007.

[31] X.D. Zhang, D.Z. Yang, J. Nie, Chitosan/polyethylene glycol diacrylate films as potential wound dressing material, Int. J. Biol. Macromol. 43 (5) (2008) 456–462, https://doi.org/10.1016/j.ijbiomac.2008.08.010.

[32] P.T.S. Kumar, S. Abhilash, K. Manzoor, S.V. Nair, H. Tamura, R. Jayakumar, Preparation and characterization of novel β-chitin/nanosilver composite scaffolds for wound dressing applications, Carbohydr. Polym. 80 (3) (2010) 761–767, https://doi.org/10.1016/j.carbpol.2009.12.024.

[33] I. Cerkez, A. Sezer, S.K. Bhullar, Fabrication and characterization of electrospun poly(e-caprolactone) fibrous membrane with antibacterial functionality, R. Soc. Open Sci. 4 (2) (2017) 8, https://doi.org/10.1098/rsos.160911.

[34] A. Abbaszadegan, Y. Ghahramani, A. Gholami, B. Hemmateenejad, S. Dorostkar, M. Nabavizadeh, H. Sharghi, The effect of charge at the surface of silver nanoparticles on antimicrobial activity against gram-positive and gram-negative bacteria: a preliminary study, J. Nanomater. 2015 (2015) 1–8, https://doi.org/10.1155/2015/720654.

[35] M. Monfared, S. Taghizadeh, A. Zare-Hoseinabadi, S.M. Mousavi, S.A. Hashemi, S. Ranjbar, A.M. Amani, Emerging frontiers in drug release control by core-shell nanofibers: a review, Drug Metab. Rev. 51 (4) (2019) 589–611, https://doi.org/10.1080/03602532.2019.1642912.

[36] Z.X. Zeng, Z.J. Li, Y.X. Zhao, J.J. Liu, J.X. Feng, Z.P. Jing, R. Feng, Endovascular repair combined with staged drainage for the treatment of infectious aortic aneurysm: a case report, BMC Cardiovasc. Disord. 20 (1) (2020) 4, https://doi.org/10.1186/s12872-020-01694-9.

[37] I. Heinola, I. Kantonen, M. Jaroma, A. Alback, P. Vikatmaa, P. Aho, M. Venermo, Editor's choice - treatment of aortic prosthesis infections by graft removal and in situ replacement with autologous femoral veins and fascial strengthening, Eur. J. Vasc. Endovasc. Surg. 51 (2) (2016) 232–239, https://doi.org/10.1016/j.ejvs.2015.09.015.

[38] J. Bernatchez, V. Gauvin, N. Gilbert, P. Rhéaume, Long-term results of the neoaortoiliac system procedure for aortic graft infections and mycotic aneurysms: a single-center experience, J. Vasc. Surg. 64 (5) (2016), https://doi.org/10.1016/j.jvs.2016.08.036.

[39] Z. Sun, E. Zussman, A.L. Yarin, J.H. Wendorff, A. Greiner, Compound core–shell polymer nanofibers by Co-electrospinning, Adv. Mater. 15 (22) (2003) 1929–1932, https://doi.org/10.1002/adma.200305136.

[40] X. Hu, S. Liu, G. Zhou, Y. Huang, Z. Xie, X. Jing, Electrospinning of polymeric nanofibers for drug delivery applications, J. Control Release 185 (2014) 12–21, https://doi.org/10.1016/j.jconrel.2014.04.018.

[41] Z. Tan, H. Wang, X. Gao, T. Liu, Y. Tan, Composite vascular grafts with high cell infiltration by co-electrospinning, Mater. Sci Eng C Mater Biol Appl 67 (2016) 369–377, https://doi.org/10.1016/j.msec.2016.05.067.

[42] Y.J. Li, F. Chen, J. Nie, D.Z. Yang, Electrospun poly(lactic acid)/chitosan core-shell structure nanofibers from homogeneous solution, Carbohydr. Polym. 90 (4) (2012) 1445–1451, https://doi.org/10.1016/j.carbpol.2012.07.013.

[43] C. Marambio-Jones, E.M.V. Hoek, A review of the antibacterial effects of silver nanomaterials and potential implications for human health and the environment, J. Nanopart. Res. 12 (5) (2010) 1531–1551, https://doi.org/10.1007/s11051-010-9900-y.

[44] M. Funovics, X. Montet, F. Reynolds, R. Weissleder, L. Josephson, Nanoparticles for the optical imaging of tumor E-selectin, Neoplasia 7 (10) (2005) 904–911, https://doi.org/10.1593/neo.05352.

[45] D. Acharya, P. Pandey, B. Mohanta, A comparative study on the antibacterial activity of different shaped silver nanoparticles, Chem. Pap. 75 (9) (2021) 4907–4915, https://doi.org/10.1007/s11696-021-01722-8.

[46] A.C. Alavarse, F.W.D. Silva, J.T. Colque, V.M. da Silva, T. Prieto, E.C. Venancio, J. J. Bonvent, Tetracycline hydrochloride-loaded electrospun nanofibers mats based on PVA and chitosan for wound dressing, Mater. Sci. Eng., C 77 (2017) 271–281, https://doi.org/10.1016/j.msec.2017.03.199.

[47] A.R. Unnithan, A.G. Nejad, A.R.K. Sasikala, R.G. Thomas, Y.Y. Jeong, P. Murugesan, S. Nasseri, D.M. Wu, C.H. Park, C.S. Kim, Electrospun zwitterionic nanofibers with in situ decelerated epithelialization property for non-adherent and easy removable wound dressing application, Chem. Eng. J. 287 (2016) 640–648, https://doi.org/10.1016/j.cej.2015.11.086.

[48] H. Yu, X.J. Chen, J. Cai, D.D. Ye, Y.X. Wu, P.F. Liu, Dual controlled release nanomicelle-in-nanofiber system for long-term antibacterial medical dressings, J. Biomater. Sci. Polym. Ed. 30 (1) (2019) 64–76, https://doi.org/10.1080/09205063.2018.1549771.

[49] K.I. Paraskevas, D.P. Mikhailidis, D. Perrea, Experimental models of abdominal aortic aneurysms: an overview, Curr. Pharm. Design 14 (4) (2008) 325–337.

[50] J. Molacek, V. Treska, J. Kobr, B. Certik, T. Skalicky, V. Kuntscher, V. Krizkova, Optimization of the model of abdominal aortic aneurysm - experiment in an animal model, J. Vasc. Res. 46 (1) (2009) 1–5, https://doi.org/10.1159/000135659.